

Ultrawide broadband rectification effect in an in-plane magnetic tunnel junction

G.A. Kichin^{1,*}, P.N. Skirdkov^{1,2} and K.A. Zvezdin^{1,2}

¹*New Spintronic Technologies, Russian Quantum Center, Bolshoy blv. 30, Moscow 121205, Russia*

²*Prokhorov General Physics Institute of the Russian Academy of Sciences, Vavilova 38, Moscow, 119991, Russia*



(Received 16 February 2023; revised 28 July 2023; accepted 12 October 2023; published 30 October 2023)

Broadband voltage rectification is an interesting effect that was recently discovered in magnetic tunnel junction (MTJ) structures. Usually, this effect occurs for certain types of MTJ structures and for special configurations of the external magnetic field (namely, perpendicular to the plane component of magnetization). We report on an alternative type of broadband rectification effect with a frequency range up to 6 GHz that is observed in MTJ samples with in-plane magnetization and without an external out-of-plane magnetic field. We compare the experimental study with numerical calculations and theoretical analysis to explain the results. Furthermore, we demonstrated that for the appearance of broadband rectification, it is sufficient to create a nonzero equilibrium angle between the polarizer and the free layer. Our work paves the way for improved energy efficiency in wireless microwave energy-harvesting applications.

DOI: 10.1103/PhysRevApplied.20.044078

I. INTRODUCTION

The widespread use of automation and Internet of Things (IoT) systems is based on the extensive use of wireless sensor nodes, which requires alternative approaches to ensure autonomous power supply. An issue here is the efficiency of the power supply of low-power edge nanodevices. One way to solve this problem is to use systems capable of collecting and harvesting energy from electromagnetic background radiation from artificial sources, such as WiFi or cellular networks. A potential solution can be offered by spintronic devices based on magnetic tunnel junction (MTJ) [1]. MTJs have shown their potential for use as memory cells [2,3], nano-oscillators [4–6], spectrum-analyzing [7] and communication devices [8], nodes for neuromorphic systems [9–11], and random-bit generators [12–14]. Recent research has revealed that these devices can convert high-frequency currents into dc voltage via the spin-torque diode (STD) rectification effect [15]. An overview of recent research in this area can be found in Refs. [16,17].

Experiments have shown that the rectification effect in MTJ has a resonant behavior and is highly efficient only near the ferromagnetic resonance (FMR). This fact creates limitations for spin-torque diode-based rf detectors. Indeed, their performance may degrade or become impractical at frequencies distant from the resonant one. This limited frequency range of efficient rectification restricts its applicability in high-frequency applications.

The first possible way to solve the problem is through frequency engineering [16] aimed at certain application. It was demonstrated that the resonant frequency can be tuned by the magnetic field [18], additional coupling [19–24], the appearance of exotic magnetic state (for example, vortex [25–27]), or/and additional bias currents [28–30].

The main pros of this approach are high sensitivity at low powers and frequency selectivity in the case of resonant rectification. State-of-the-art MTJs significantly outperform conventional Schottky diodes in terms of microwave sensitivity in a power range below 1 μW [28–30]. The record-breaking results on microwave sensitivity have been achieved due to the presence of perpendicular magnetic anisotropy, additional bias current, and even injection locking between the dc driven self-oscillation and microwave input signal that provides a high-amplitude out-of-plane precession [28–30]. Even without dc bias, the presence of perpendicular magnetic anisotropy can cause a high-amplitude out-of-plane precession with record-breaking passive microwave sensitivity [29–32].

The frequency-engineering approach, however, also has some cons. For many applications, frequency selectivity is a weakness. Moreover, the precise technological control of MTJ's parameters required for frequency engineering is rather difficult or sometimes even not possible.

Recently, another type of rectification regime has been reported in a theoretical paper [33]. The rectified voltage was observed in a very wide frequency range and did not have a resonant character. This broadband rectification was attributed to a large-angle out-of-plane (OOP) precession of the free-layer magnetization. A necessary condition for this regime is a significant OOP component of the

* g.kichin@nst.tech

magnetization at the equilibrium state (so-called easy-cone state). The OOP component was originally proposed to be created using perpendicular magnetic field bias [33]. However, recent findings have shown that it is possible to create an OOP magnetization component using interfacial PMA [34–36]. For example, Fang *et al.* [34] have used the MTJ samples designed to have a free-layer thickness near, but below, this critical value, so that the PMA field almost compensates for the out-of-plane demagnetizing field. Tarequzzaman *et al.* [35] have studied the emergence of broadband rectification in MTJ with the perpendicular magnetic anisotropy (PMA) component of the magnetization by tailoring the thickness of the free layer during the manufacturing process. Up until today, through free-layer proper interface PMA engineering, the maximum bandwidth of the broadband STD detection was reported to be up to 3 GHz [37]. Also, it has been shown that the operation of the MTJs as rf detector in a broadband regime is observed only when a certain power threshold is exceeded [34,37]. The broadband mode shown in Ref. [35] has a nearly zero-power threshold because of a smooth linear resistance dependency in the MTJs used in measurements, however this STD design suffers from the much narrower frequency band. Later, it has been shown theoretically [38] that the devices with wider frequency bands have a larger threshold power value. Although the mentioned results on broadband rectification are very promising from the applied point of view, the required fine tuning of the perpendicular magnetic anisotropy increases the technical complexity of their implementation.

In this paper, we report an alternative type of nonresonant, broadband RF rectification mechanism in MTJs with in-plane magnetization of the free layer. We analyze how

the rectification effect depends on the direction of the in-plane external magnetic field and the input radio frequency power. Using the spin-torque FMR (ST FMR) method, we show that spin-torque driven responses exhibit rf rectification over a very wide frequency range, reaching a record-breaking 6 GHz. We propose the analytical model and perform micromagnetic simulations to get a theoretical insight into the magnetization dynamics behind the experimentally observed wide-range rectification effect. We have found that the deviation of the in-plane magnetization orientation in the free layer regarding the direction of the magnetization of the polarizer, caused by the in-plane external magnetic field, plays the key role in the observed effect.

II. EXPERIMENT

We consider the magnetic tunnel junction (MTJ) with the following structure (from bottom to top): Ta(3 nm)/PtMn(15 nm)/Co₇₀Fe₃₀(2.5 nm)/Ru(0.85 nm)/Co₆₀Fe₂₀B₂₀(2.9 nm)/Co₇₀Fe₃₀(0.4 nm)/MgO(1 nm)/Co₇₀Fe₃₀(0.4 nm)/Co₆₀Fe₂₀B₂₀(1.6 nm)/Ta(5 nm)/Ru(7 nm) which is similar to structures from Ref. [18,39]. The MTJ stack is patterned into an elliptical shape with axes of 250 × 50 nm² [see Fig. 1(a)]. The sample was annealed at 360°C in a 1-T magnetic field for 1 h. The bilayer Co₇₀Fe₃₀/Co₆₀Fe₂₀B₂₀ above the MgO layer acts as a free layer in which the magnetization dynamics can be exerted. The top ferromagnetic layer of the synthetic antiferromagnetic (SAF) structure Co₇₀Fe₃₀/Ru/Co₆₀Fe₂₀B₂₀/Co₇₀Fe₃₀ below MgO acts as a pinned layer (or polarizer) with fixed in-plane oriented magnetization (along the large ellipse axis).

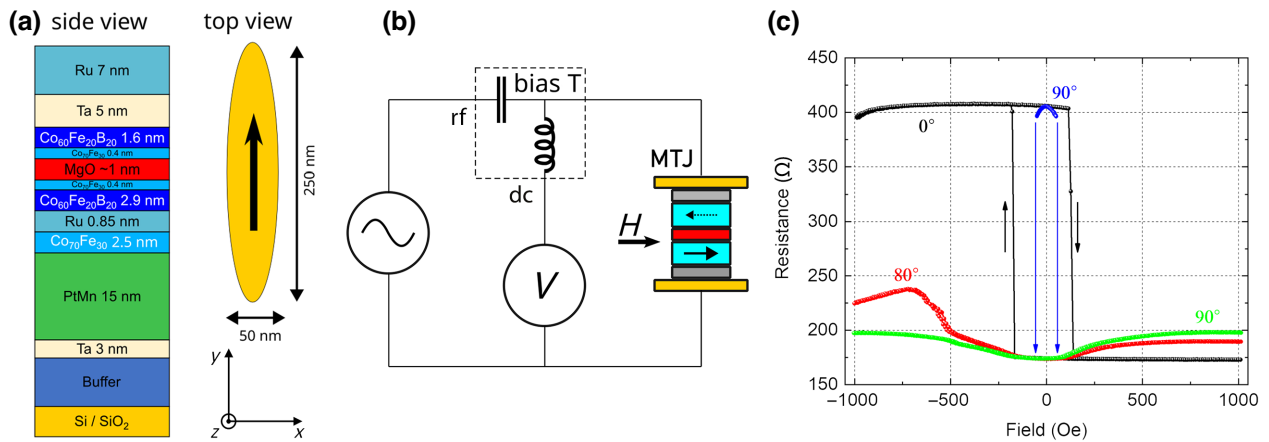


FIG. 1. (a) Cross-section view and lateral dimensions of the MTJ sample with Cartesian coordinate system. (b) Sketch of the ST FMR setup with an external magnetic field applied along the easy axis from the pinned-layer magnetization. (c) Magnetoresistance as a function of the in-plane magnetic field for elliptical MTJ nanopillar (250 × 50 nm²). The black curve is for a magnetic field oriented parallel to the easy axis of the pinned layer. The black arrows indicate the magnetic field sweep direction. The blue and green curves relate to the cases of the magnetic field perpendicular to the easy axis of the pinned layer. The blue curve is for the sample initially set to AP state. Blue arrows show a drop of magnetoresistance from high value to low value because of the AP to P transition. The red curve is for the field applied at 80° degrees to the easy axis of the pinned layer.

Initially, we characterized the resistance of the sample as a function of the magnetic field. The external magnetic field is oriented toward the easy axis of the pinned layer. The sign of the field is chosen to set the sample into a parallel (P) state for high positive field values. In the P state, the sample has resistance $R_P = 173 \Omega$. For large negative field values, the sample is in the antiparallel (AP) state with $R_{AP} = 407 \Omega$. TMR value is about 135%. The magnetization switching from the AP state to the P state occurs at a field value of 160 Oe, and from the P state to the AP state at -285 Oe. A steplike switching shows a high-quality manufacturing process of the pinned and free layers and high uniformity of the magnetization in these layers near the switching point. In large negative fields (below -1100 Oe), the SAF starts switching. The SAF switching has also a hysteresis behavior with a loop width of about 209 Oe.

To analyze the influence of field angle we also measured MTJ resistance dependencies on the field for two additional angles: 80° and 90° to the polarizer direction. All hysteresses for 0°, 80°, and 90° are presented in Fig. 1(c). All results are obtained with a probing current $I_{dc} = 50 \mu\text{A}$.

To study the possibility of broadband rectification in the sample with in-plane magnetization, the sample was placed in a planar magnetic field. The rectified voltage for different field orientations is measured using the ST FMR

technique [40–42]. The experimental setup scheme is presented in Fig. 1(b). Rectified dc voltage was detected using the high-precision source-measurement unit NI 4137. A Keysight 5173B generator was used as the rf source. rf signal power was 0.1 mW (-10 dBm). Rectified dc and rf signals were separated using a bias tee (Mini-Circuits ZFBT-6GW). The bottom contact of the MTJ was grounded. The rotation of the external in-plane field was carried out by using an electromagnet positioned on the PC-controlled rotating platform. The experiment was performed at room temperature. The colormaps of rectified voltage dependence on frequency and field value $U(f, H)$ for different field angles (0°, 80°, and 180°) are presented in Figs. 2(a), 2(b), 2(c). The spectra of rectified voltage for several field values and different field angles (0°, 80°, and 180°) are presented in Figs. 2(d), 2(e), 2(f). For the magnetic field value of -1000 Oe, the MTJ sample is in the AP state for 0° and in the P state for 180°.

For a field direction 180° and for a field magnitude range -1000 Oe to 0 Oe, there is a minor change in the rectified voltage. There is a light blue area in Fig. 2(c). There are no features on the colormap we can observe. For a detailed view, we plot several individual spectra for this case [see Fig. 2(f)]. The rectified voltage value reaches $|V| = 0.2$ mV at the 0.5 GHz end of the spectrum and 0.04 mV at the 6 GHz end of the spectrum. The average value is estimated as 0.05 mV.

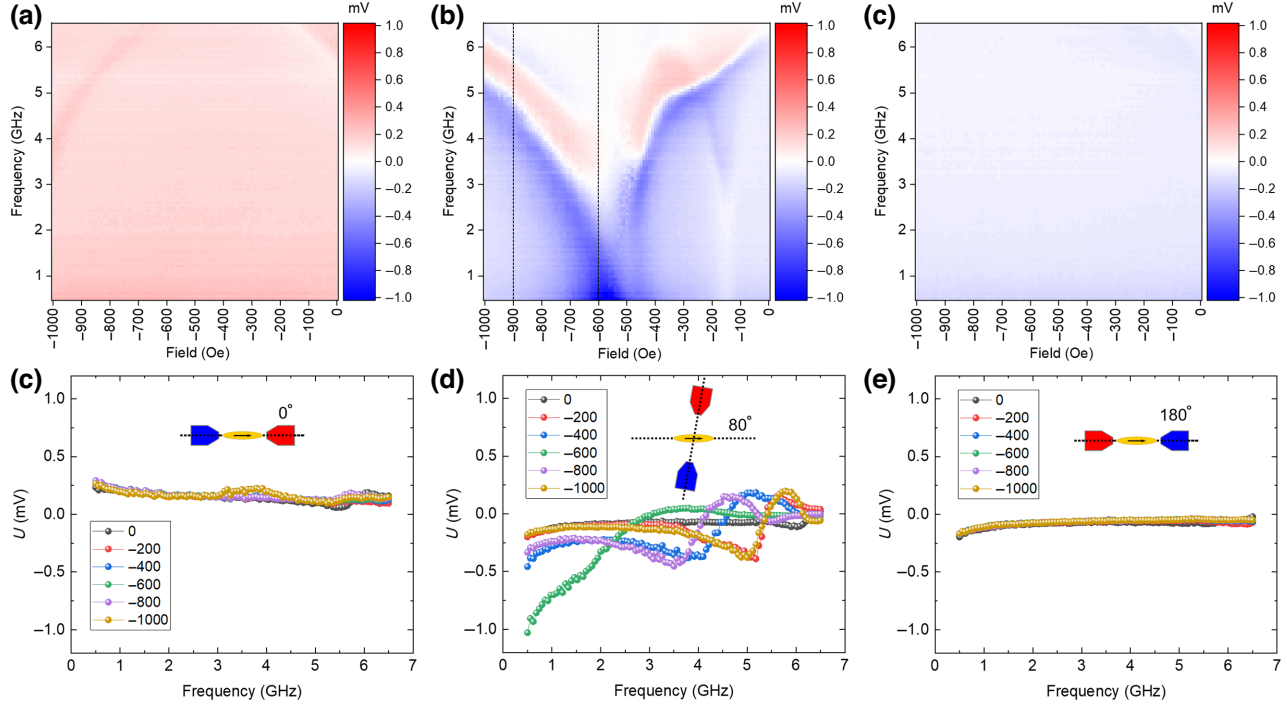


FIG. 2. Rectified voltage for different magnetic field directions: (a) field is applied along the polarizer direction (0°), (b) field is applied at an 80° degree to the polarizer direction, (c) field is applied opposite to the polarizer direction (180°). Set of spectra for different field values from the range -1000 to 0 Oe and for different directions: (d) 0°, (e) 80°, and (f) 180°. The orientations of the electromagnet, polarizer, and sample are presented in insets.

For the field direction 0° and field range from -1000 Oe to 0 Oe the magnitude of the rectified voltage also does not change significantly. However, now there are some weak resonant-like modes in the map [see Fig. 2(a)]. The observable part of one mode starts at 0 -Oe field at 5 GHz and ends at -200 Oe at 6.5 GHz, the other mode starts at -1000 Oe at 4 GHz and ends at -700 Oe at 6.5 GHz. For a better view of the amplitude of the modes, the individual spectra of rectified voltage are plotted separately in Fig. 2(d). As in the previous case, the average value of the rectified voltage does not change a lot for MTJ in AP state. The average value of rectified voltage is $|V| = 0.15$ mV (0.3 mV at 0.5 GHz and 0.12 mV at 6.5 GHz).

A different situation occurs when the magnetic field is oriented at some angle with respect to the easy axis. The rectified voltage value increases significantly. Figure 2(b) shows the case when the field is applied at 80° to the polarizer direction. There is a pair of bright resonantlike modes in the colormap. Both modes start at -500 Oe and 0.5 GHz and one ends at -1000 Oe and 6.5 GHz while the second ends at 0 Oe, 6.5 GHz. There is also an additional second pair of modes that start at -150 Oe and 0.5 GHz. However, the rectification effect associated with them is quite weak. The analysis of the individual spectra [see Fig. 2(e)] shows a significant increase in the rectified voltage value up to 0.3 – 1 mV. The value of the rectified voltage increases significantly not only near resonances but over the entire frequency range, including an increase in the low-frequency region. Experimental results demonstrate that rectification occurs in a wide frequency range up to 6 GHz [see Figs. 2(b), 2(e)], which is much more than previously reported. Since a significant value of the rectified voltage is observed in the entire frequency range from low frequencies up to the FMR peak, this allows us to speak about the broadband rectification character of the MTJ.

It is well known that broadband rectification mode should have some power threshold [33,34]. To check its

existence, we performed additional experiments with different input radiofrequency signal powers. We focused on the case of an 80° field angle and chose two field values: -900 and -600 Oe [see two black dashed lines on Fig. 2(b)]. Sensitivity dependencies on frequency for these two field values and different input powers from -10 down to -35 dBm are presented in Fig. 3. As one can see, the sensitivity, which can be defined as rectified voltage divided by input signal power, remains the same with power variations from 0.1 mW down to 316 nW. Therefore, there is no threshold in the considered power range, and rectified voltage both in resonance and far away from it just linearly decreases with power decrease. It contrasts with previously reported broadband mode behavior [33,34] and is similar to conventional ST FMR resonance properties.

III. ANALYTICAL MODEL

For an analytical insight into reported experimental results, let us consider MTJ in macrospin approximation. We will take into account only free-layer dynamics with assumption that its magnetization distribution is always uniform. In this case, we can reduce the situation to considering the free layer as a single magnetic moment vector. To describe its dynamics let us consider Landau-Lifshitz-Gilbert-Slonczewski equation (LLGS) [43,44] in spherical coordinates (θ and φ are the azimuth and polar angles, respectively):

$$\sin \theta \frac{\partial \varphi}{\partial t} - \alpha \frac{\partial \theta}{\partial t} = \frac{\gamma}{M_S} \frac{\delta \varepsilon}{\delta \theta} + (\mathbf{p}, \mathbf{T}_\theta), \quad (1)$$

$$\sin \theta \frac{\partial \theta}{\partial t} + \alpha \sin^2 \theta \frac{\partial \varphi}{\partial t} = -\frac{\gamma}{M_S} \frac{\delta \varepsilon}{\delta \varphi} + (\mathbf{p}, \mathbf{T}_\varphi), \quad (2)$$

where where $\mathbf{m} = (\sin \theta \cos \varphi, \sin \theta \sin \varphi, \cos \theta)^T$ is the unit vector of free-layer magnetization, γ is the gyromagnetic ratio, α is the Gilbert-damping parameter, and ε is the sum of demagnetization (magnetostatic)

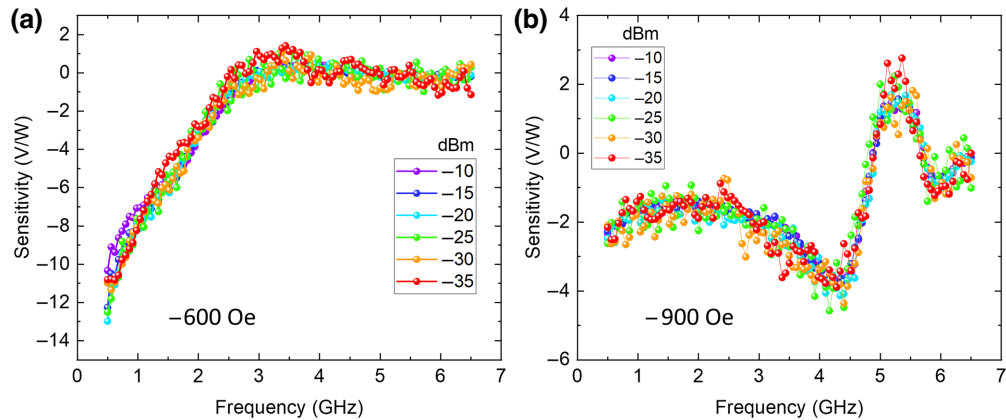


FIG. 3. Sensitivity dependencies on frequency for an 80° field angle, (a) -600 Oe and (b) -900 Oe magnetic field value and different input power from -10 dBm down to -35 dBm.

$\varepsilon_{\text{demag}}$ and Zeeman ε_H energy density. The first one can be written in the form $\varepsilon_{\text{demag}} = \frac{1}{2}N_xM_S^2m_x^2 + \frac{1}{2}N_yM_S^2m_y^2 + \frac{1}{2}N_zM_S^2m_z^2$, where M_S is saturation magnetization and N_i is demagnetization factors. However, for thin ferromagnetic layers usually $N_z \gg N_x, N_y$, and energy can be reduced to $\varepsilon_{\text{demag}} \approx 2\pi M_S^2 \cos^2 \theta + \frac{1}{2}(N_x - N_y)M_S^2 \sin^2 \theta \cos^2 \varphi$. Zeeman energy in the case of external magnetic field $\mathbf{H} = (H \cos \varphi_H, H \sin \varphi_H, 0)$ can be represented as $\varepsilon_H = -HM_S \cos \varphi_H \sin \theta \cos \varphi - HM_S \sin \varphi_H \sin \theta \sin \varphi$. Here we consider y -axis polarizer direction, i.e., $\mathbf{p} = (0, 1, 0)^T$. In this case torques will have the following forms: $(\mathbf{p}, \mathbf{T}_\theta) = \gamma a_J \cos \varphi - \gamma b_J \cos \theta \sin \varphi$ and $(\mathbf{p}, \mathbf{T}_\varphi) = \gamma a_J \sin \theta \cos \theta \sin \varphi + \gamma b_J \sin \theta \cos \varphi$, where $a_J = a_J^0 j_0 \sin(\omega t)$, $b_J = b_J^0 j_0 \sin(\omega t)$, $a_J^0 = \hbar P/(2ceM_S)$, where P is spin polarization of electrical current, $j = j_0 \sin(\omega t)$ is current density, c is the thickness of the free layer, e is the charge of the electron. The amplitude of the fieldlike torque is given by $b_J^0 = \xi_{\text{CPP}} a_J^0$, where ξ_{CPP} was chosen to be 0.4.

First, let us consider the equilibrium position (φ_0, θ_0) of the system. The form of ε leads to the following implicit solution:

$$\theta_0 = \pi/2, \quad (3)$$

$$\sin(\varphi_0 - \varphi_H) = \frac{(N_x - N_y)M_S}{2H} \sin 2\varphi_0. \quad (4)$$

This solution corresponds to the case of magnetization in a plane ($\theta_0 = \pi/2$) directed at some angle $\varphi_0 - \varphi_H$ to the external magnetic field. In the case of the round sample $N_x = N_y$ and $\varphi_0 = \varphi_H$.

Now let us consider low-amplitude dynamics in the vicinity of the found equilibrium position (φ_0, θ_0) . To do this, we write $\varphi = \varphi_0 + \varphi_1$ and $\theta = \pi/2 - \theta_1$, where $\varphi_1, \theta_1 \ll 1$. Then, neglecting small quantities, Eqs. (1) and (2) lead to

$$\begin{aligned} \frac{\partial \varphi_1}{\partial t} &= \alpha \gamma ((N_x - N_y)M_S \cos 2\varphi_0 - H \cos(\varphi_0 - \varphi_H)) \varphi_1 \\ &+ \gamma ((N_x - N_y)M_S \cos^2 \varphi_0 - H \cos(\varphi_0 - \varphi_H) \\ &- 4\pi M_S) \theta_1 + \gamma (a_J^0 + \alpha b_J^0) j_0 \cos \varphi_0, \end{aligned} \quad (5)$$

$$\begin{aligned} \frac{\partial \theta_1}{\partial t} &= \gamma (H \cos(\varphi_0 - \varphi_H) - (N_x - N_y)M_S \cos 2\varphi_0) \varphi_1 \\ &+ \alpha \gamma ((N_x - N_y)M_S \cos^2 \varphi_0 - H \cos(\varphi_0 - \varphi_H)) \theta_1 \\ &+ \gamma (\alpha a_J^0 - b_J^0) j_0 \cos \varphi_0. \end{aligned} \quad (6)$$

Let us first consider a homogeneous system. For it, the dependence of the resonant frequency after expanding with respect to a small parameter $(N_x - N_y)M_S/H \ll 1$ and neglecting small values can be written in the form:

$$\begin{aligned} \omega_0^2 &= \gamma \left[H \left(H + 4\pi M_S \left(1 - \frac{N_x - N_y}{8\pi} (1 + 3 \cos 2\varphi_0) \right) \right) \right. \\ &\quad \left. - 4\pi M_S^2 (N_x - N_y) \cos 2\varphi_0 \right]. \end{aligned} \quad (7)$$

As one can see, this equation takes the form of a typical Kittel dependence $\omega_0^2 = \gamma^2 H (H + 4\pi M_S)$ in the case of $N_x = N_y$.

Now we will consider the inhomogeneous system of Eqs. (5) and (6). Let us pass to the Fourier space and look for a solution in the form of harmonic functions $\varphi_1(t) = \tilde{\varphi}_1(\omega)e^{-i\omega t}$ and $\theta_1(t) = \tilde{\theta}_1(\omega)e^{-i\omega t}$. To get rid of cumbersome calculations, consider the case of a round sample $N_x = N_y$. In this case, in what follows, to take into account the effect of ellipticity, we will use solutions for a round disk, in which, however, instead of the true field angle φ_H , the equilibrium angle φ_0 obtained from Eq. (4) will be used as a field angle. In the approximation of small oscillations and for high field values $((N_x - N_y)M_S/H \ll 1)$, this approach will allow us to accurately take into account the ellipticity, since for such a case, the presence of ellipticity will only slightly change the equilibrium direction of magnetization. Then the system of Eqs. (5) and (6) can be rewritten as

$$\begin{aligned} -i\omega \tilde{\varphi}_1 &= -\alpha \gamma H \tilde{\varphi}_1 - (\gamma H + 4\pi \gamma M_S) \tilde{\theta}_1 \\ &+ \gamma (a_J^0 + \alpha b_J^0) j_0 \cos \varphi_0, \end{aligned} \quad (8)$$

$$-i\omega \tilde{\theta}_1 = \gamma H \tilde{\varphi}_1 - \alpha \gamma H \tilde{\theta}_1 + \gamma (\alpha a_J^0 - b_J^0) j_0 \cos \varphi_0. \quad (9)$$

From this system of equations one can derive

$$\tilde{\varphi}_1 = -\frac{(\gamma(i\omega - \Gamma)(a_J^0 + \alpha b_J^0) + \omega_0^2(\alpha a_J^0 - b_J^0)/H) (\omega_0^2 - \omega^2 + \Gamma^2 + 2i\omega\Gamma)}{(\omega_0^2 - \omega^2 + \Gamma^2)^2 + 4\omega^2\Gamma^2} j_0 \cos \varphi_0, \quad (10)$$

where $\Gamma = \alpha \gamma H$. It is well known that the macrospin model tends to overestimate the resonance peaks [45]. Foremost, this is due to the fact that this model only

describes the dynamics of uniform magnetization. At the same time, in reality, at resonance, the excitation efficiency becomes very high, which also leads to the excitation of

non-uniform oscillations. Often this effect is called inhomogeneous broadening, and in many models (for example, for the FMR experiment), an empirical inhomogeneous broadening ΔH_0 is added, which is equivalent to additional damping. Similarly, to limit the peak values in the macrospin model, we add an additional inhomogeneous damping in the form $\alpha = \alpha_0 + \alpha_{\text{inh}}$.

Now, to calculate the rectified voltage, we write the MTJ resistance in the form $R = R_P + \Delta R(1 - \mathbf{m} \cdot \mathbf{p})/2 = R_P + \Delta R(1 - \sin(\varphi_0 + \varphi_1))/2 \approx R_P + \Delta R(1 - \sin \varphi_0 - \varphi_1 \cos \varphi_0)/2$, where $\Delta R = R_{AP} - R_P$. The mean voltage can be calculated as $\langle U \rangle = 1/T \int_T \text{Re}\{IR\}dt = -\Delta RI_0/(4) \cos \varphi_0 \times \text{Re}\{\tilde{\varphi}_1\}$, where $I_0 = j_0 S$ and S is the MTJ area. Neglecting small values ($\alpha \ll 1$) one can write down the final expression of rectified voltage:

$$\langle U \rangle = -\frac{I_0^2 \Delta R \gamma}{4S\Gamma} \cos^2 \varphi_0 \times \frac{(\Gamma^2 a_J^0 - \alpha \omega_0^2 b_J^0) \omega^2 + \Gamma^4 a_J^0 + \alpha \omega_0^4 b_J^0}{(\omega_0^2 - \omega^2 + \Gamma^2)^2 + 4\omega^2 \Gamma^2}. \quad (11)$$

We will use the following system parameters corresponding to our experimental data and typical material properties: $S = \pi ab$, $a = 125$ nm, $b = 25$ nm, $j_0 = 4 \times 10^6$ A/cm² (which corresponds to -10 dBm), $\Delta R = 225$ Ω, $\alpha = 0.3$ (already with additional inhomogeneous damping), $H = 420$ Oe, $a_J^0 = 5.5 \times 10^{-6}$ Oe/(A/cm²), $b_J^0 = 2.2 \times 10^{-6}$ Oe/(A/cm²), $M_S = 950$ emu/cm³, $N_x = 0.066 \times 4\pi$, and $N_y = 0.011 \times 4\pi$. The dependence of the rectified voltage on the frequency, obtained by Eq. (11), for the cases of field angles 0° , 80° , 90° , and 100° is shown in Fig. 4. As can be seen from these results, the macrospin

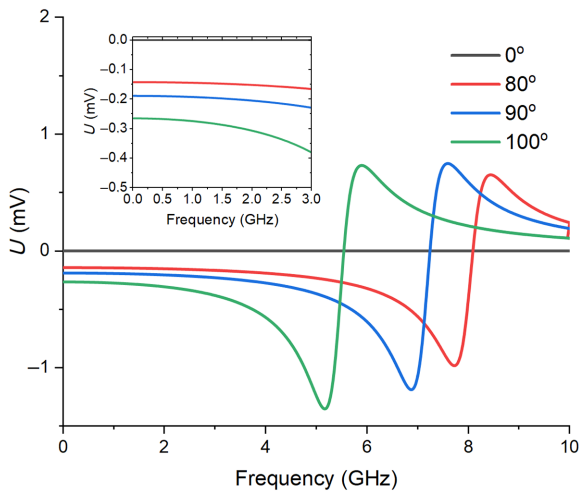


FIG. 4. Rectified voltage dependence on the frequency, obtained by Eq. (11), for the cases of field angles 0° , 80° , 90° , and 100° . The frequency range from 0 to 3 GHz with increase is shown in the inset.

model reproduces broadband rectification from zero to ferromagnetic resonance frequencies at nonzero field angles. At the same time, its value is similar to the value in the experiment. This fact confirms the magnetic nature of the effect observed in the experiment, which, however, can be amplified by $1/f$ noise at low frequencies. Also, Eq. (11) clearly shows that the observed broadband rectification is not separable from the FMR peak, and appears due to its deformation. Another interesting fact is that the rectified voltage in Eq. (11) clearly depends ($\langle U \rangle \sim \cos^2 \varphi_0$) on the angle φ_0 , which is related to the angle ϕ between the free layer and the polarizer by the expression $\phi = \pi/2 - \varphi_0$. This fact indicates that a nonzero angle between the free layer and the polarizer is a necessary condition for the occurrence of broadband rectification ($\langle U \rangle \sim \sin^2 \phi$). However, to accurately test this hypothesis, it is also necessary to take into account all the nonuniformities and the dynamics of the polarizer, which is possible only in micromagnetic modeling.

IV. MICROMAGNETIC MODELING

For macrospin model results verification we performed micromagnetic simulations of the considered system. In general, the magnetization dynamics in ferromagnetic layers is described by the Landau-Lifshitz-Gilbert-Slonczewski equation (LLGS) [43,44]:

$$\frac{d\mathbf{m}_i}{dt} = -\gamma \mathbf{m}_i \times \mathbf{H}_i^{\text{eff}} + \alpha \mathbf{m}_i \times \frac{d\mathbf{m}_i}{dt} + \mathbf{T}_{\text{STT}}^i, \quad (12)$$

i is the index of the ferromagnetic layer (1 is for free layer, 2 is for polarizer, and 3 is for fixed layer), \mathbf{m}_i is the unit vector of magnetization of the i th layer, $\mathbf{H}_i^{\text{eff}}$ is the effective magnetic field of the i th layer. In Eq. (12), the effective magnetic field can be calculated as $\mathbf{H}_i^{\text{eff}} = -\delta E/\delta \mathbf{M}_i$, where E is the sum of magnetostatic energy, exchange energy, anisotropy energy, and effective antiferromagnetic interlayer exchange energy. The spin-transfer torque in Eq. (12) is represented by the sum of two components $\mathbf{T}_{\text{STT}}^i = \mathbf{T}_{\text{ST}}^i + \mathbf{T}_{\text{FLT}}^i$, where $\mathbf{T}_{\text{ST}}^i = -\gamma a_J^i \mathbf{m}_i \times (\mathbf{p}_i \times \mathbf{m}_i)$ is Slonczewski torque, $\mathbf{T}_{\text{FLT}}^i = -\gamma b_J^i \mathbf{p}_i \times \mathbf{m}_i$ is fieldlike torque, \mathbf{p}_i is the unit vector of magnetization in the layer, which creates polarization. For the free layer \mathbf{p}_i is defined by polarizer layer, for the polarizer by the free layer. The Slonczewski torque has an amplitude $a_J^i = \hbar P/(2c_i e M_s^i)$, where P is spin polarization of electrical current, c_i is the thickness of the corresponding layer, M_s^i is the corresponding magnetization saturation, e is the charge of the electron. The amplitude of the fieldlike torque is given by $b_J^i = \xi_{\text{CPP}} a_J^i$, where ξ_{CPP} was chosen to be 0.4 similarly to the macrospin case.

For the numerical integration of the LLGS equation, we use our micromagnetic finite-difference code SpinPM, which is based on the fourth-order Runge-Kutta method

with an adaptive timestep control for the time integration and a mesh size of $2 \times 2 \times c_l$ nm³. Using it, we perform a series of simulations of the full MTJ structure, including free layer and SAF (consisting of polarizer and fixed layer), with dynamic calculation of full magnetostatic and STT in both free and polarizer layers.

We consider MTJ with similar to experimental geometrical parameters and layer thicknesses and materials. All the resistance parameters were chosen due to experimental data: $\Delta R = 225$ Ω, $R_P = 173$ Ω, and $R_{AP} = 407$ Ω. We consider ruthenium interlayer exchange constant $J_{ex}^{\text{Ru}} = -0.13$ (erg/cm²), ferromagnetic layer exchange constants $A_{ex} = 1.6 \times 10^{-6}$ (erg/cm), and Gilbert damping $\alpha = 0.01$. Magnetic crystalline anisotropy was assumed to be zero $K = 0$. Spin polarization $P = 0.4$. Magnetization saturation was $M_S^{\text{free}} = M_S^{\text{pol}} = 1100$ emu/cm³ for free layer and polarizer and $M_S^{\text{fix}} = 1200$ emu/cm³ for the second (CoFe) ferromagnetic layer of the SAF. The fixed layer also experienced pinning field 20 kOe, which models the exchange interaction with PtMn layer.

ac density flowing through the spin-torque diode is equal to $j(t) = j_0 \times \sin(2\pi ft)$, j_0 is the amplitude of the ac density, which was selected to match -10 dBm input power, f is the frequency of the ac. We assume that the spin-torque diodes are connected to the power source via $Z_0 = 50$ Ω transmission line, which results in a reflection of part of the incident incoming power P_{in} . Power consumed by the diode P_{diode} can be estimated with the telegraph equation as $P_{diode} \approx 4\bar{R}Z_0P_{in}/(\bar{R} + Z_0)^2$, where $\bar{R} = 2/(R_{AP}^{-1} + R_P^{-1})$ is the average diode resistance. Taking into account magnetoresistance of magnetic tunnel junction $R(t) = R_P + \Delta R/2(1 - \mathbf{m}_{\text{free}}(t) \cdot \mathbf{m}_{\text{pol}}(t))$, one can calculate rectified voltage $V_{diode} = \langle j(t)SR(t) \rangle$ and power consumed by STD $P_{diode} = 4\bar{R}Z_0/(\bar{R} + Z_0)^2 \langle j^2(t)S^2R(t) \rangle$.

First, we perform static analysis by considering -100, -300, and -500 Oe external fields with different directions and analyzing the magnetization directions of free and polarizer layers. The results are presented in Fig. 5. We start with the AP configuration and then, with increasing field angles, the magnetization directions of both layers change. The value $\sin^2 \phi$ (which is proportional to rectified voltage $\langle U \rangle$ according to the analytical model) is zero in parallel and antiparallel orientations and has a maximum when the external field is almost perpendicular (see inset in Fig. 5). It is also worth noting that the effect of nonuniformity of magnetization can be neglected since in all simulations it occurs to be less than 0.2%, which additionally substantiates the analytical model constructed above.

After that, we perform simulations for several current frequencies in the case of -500 Oe external field directed at the angles 0°, 80°, 90°, and 100°. The rectified voltage is presented on Fig. 6. Modeling shows that the polarizer oscillation amplitude is about 5–6% of free layer's magnetization amplitude dynamics, therefore

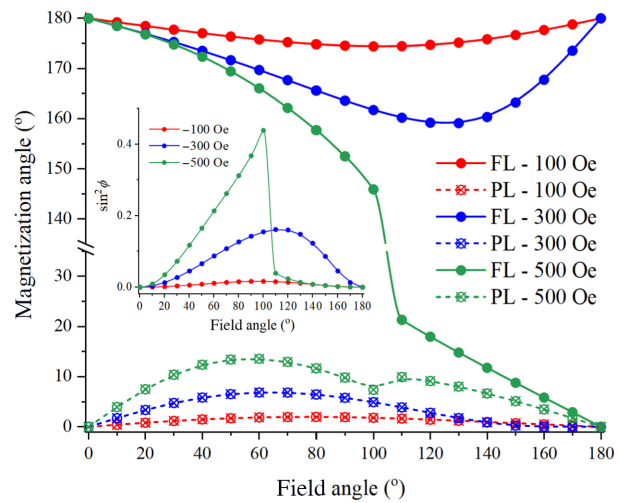


FIG. 5. Magnetization angle of the free layer and polarizer in the case of different external field value and direction obtained by micromagnetic modeling. Inset: the dependence of $\sin^2 \phi$ on external field angle for different field values.

the major effect is caused by the free-layer dynamics. This fact once again confirms the correctness of the constructed macrospin model. As one can see, the resulting voltage is nonzero in the area from zero up to the FMR resonant frequency. The existence of a rectified voltage comparable both to the experimental one and to the analytical macrospin model in the similar frequency range proves our explanation of the mechanism of the reported broadband mode. Since our micromagnetic simulations do not consider noises and measuring device features, modeling results also prove the magnetic nature of the

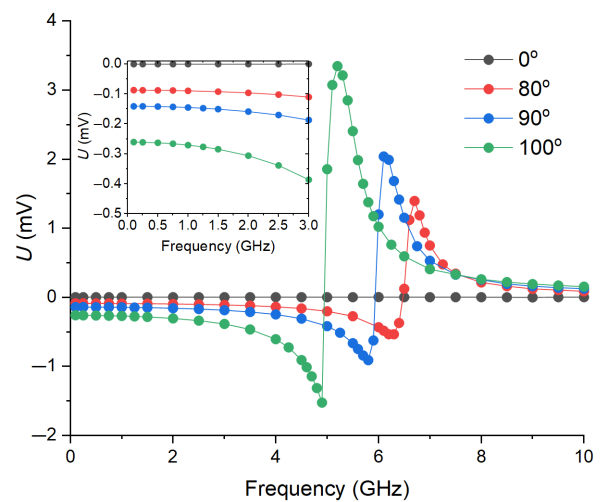


FIG. 6. Rectified voltage dependence on the frequency, obtained by micromagnetic modeling, for the cases of field angles 0°, 80°, 90°, and 100°. The frequency range from 0 to 3 GHz with increase is shown in the inset.

reported effect, which, however, can be supplemented by an electrical $1/f$ noise effect at low frequencies.

V. DISCUSSION

To better describe the reported effect, it is first worth trying to discuss the general meaning of the term broadband rectification mode. Intuitively, one would like to define this regime as the one with an approximately constant rectified voltage as a function of frequency, what implicitly implies no resonant dependence. However, according to the original work [33] in the broadband mode, “the output voltage of an spin-torque microwave detector increases with the frequency of the input signal.” Moreover, the typical experimental demonstration [34] of broadband rectification in MTJ with perpendicular anisotropy also does not demonstrate constant voltage, which in reality varies several times in the frequency range of broadband rectification. In this regard, it is more reasonable to look at the broadband mode as a mode in which there is a nonzero rectification of a similar order in magnitude over a wide frequency range.

Another issue is the difference between broadband and resonant FMR modes. From the point of view of practical application, these modes are certainly fundamentally different. However, from the point of view of the physics behind them, they are largely of a similar nature and can continuously transform into each other. For example, the application of a bias current in work [30] causes the resonance to broaden up to 0.5 GHz, effectively driving the system continuously from resonant to broadband rectification. At the same time, in work [34], in almost all rectification spectra, the broadband mode is limited from above in frequency by the resonant peak, which cannot be clearly separated from the broadband rectification region. As a result, both the resonant mode and broadband mode are special cases of the general solution of an oscillatory system, and are present simultaneously. In support of this, our analytical model and our micromagnetic simulation both exhibit both a resonant peak and broadband rectification.

At the same time, it should be noted that in most works, broadband rectification mode is understood as broadband rectification mode with large-amplitude out-of-plane precession. This mode typically requires overcoming some power threshold to drive the mentioned large-amplitude out-of-plane precession [34,37]. However, this requirement is necessary primarily to achieve high-amplitude precession, and not for the appearance of broadband rectification. In our work, we show that broadband STD rectification is a more general effect than the previously reported one, and is possible without excitation of large-amplitude out-of-plane precession. This explains the absence of a power threshold in our experiments.

However, if the amplitude of the oscillations of the magnetization is small, the broadband rectification may be lower in magnitude than the measurement device detectivity. As a result, in such an experiment, a conventional FMR peak of in-plane MTJ will be obtained without any broadband mode. For example, our rectification experimental results in the case of 0° and 180° field angles [see Figs. 2(d) and 2(f)] are similar to conventional ST FMR resonance properties of in-plane MTJ. All nonzero rectification in this case can be attributed to $1/f$ noise, which switch its sign with transition from AP state to P state. At the same time, for broadband rectification with large-amplitude out-of-plane precession, the nonzero angle of magnetization exit from the plane [33] plays a critical role in increasing the voltage values. In fact, the out-of-plane angle in that system is the angle between the magnetization of the free layer and the polarizer. In our work, we show both experimentally and theoretically that the presence of a nonzero angle between the magnetizations of the free layer and the polarizer, even in the plane, also leads to the appearance of broadband rectification [see Fig. 2(e)]. And although its value (and therefore power conversion) turned out to be several times lower (peak rf-to-dc conversion efficiency in our case is about $4.5 \times 10^{-3}\%$ at 0.1 mW) than previously reported in the case of large-amplitude out-of-plane precession [34], this result shows the possibility of an alternative approach to the broadband mode that does not require perpendicular magnetic anisotropy. Moreover, in terms of power-conversion efficiency per area our results comparable to the Schottky diodes (SMS7630), due to area difference. The area of Schottky diodes and MTJs are 10 and $9.8 \times 10^{-3} \mu\text{m}^2$, respectively. It is worthwhile to note, a similar mechanism can be implemented without an external field, which, like PMA, is a technological limitation. It is sufficient to create a nonzero equilibrium angle between the polarizer and the free layer, which, for example, can be achieved by annealing of the polarizer in the field at an angle to the major axis of the ellipse.

VI. SUMMARY AND CONCLUSIONS

In this work we report an alternative spin-torque broadband rectification effect, the mechanism of which is based on the appearance of an in-plane angle between the magnetizations of the free layer and the polarizer. We show that an external in-plane magnetic field oriented at some angle to the easy axis of the free layer of MTJ significantly improves the rectified voltage output. We use the ST FMR method to measure the rectified voltage as a function of the frequency of the input signal and the applied magnetic field. A strong increase in rectified dc voltage can be observed over a wide frequency range, from fractions of a GHz to a record 6 GHz, which is much more than previously reported. In addition, we present analytical marcospin model and micromagnetic simulations, which

provide insight into the dynamics of the system's magnetization, reveal the role played by turned magnetic field and proves the magnetic nature of the reported effect. Our work paves the way towards improved energy efficiency of wireless microwave energy-harvesting applications.

ACKNOWLEDGMENTS

Financial support by the Russian Science Foundation, Project No. 19-12-00432 is gratefully acknowledged.

- [1] S. Yuasa, T. Nagahama, A. Fukushima, Y. Suzuki, and K. Ando, Giant room-temperature magnetoresistance in single-crystal Fe/MgO/Fe magnetic tunnel junctions, *Nat. Mater.* **3**, 868 (2004).
- [2] B. N. Engel, J. Akerman, B. Butcher, R. W. Dave, M. DeHerrera, M. Durlam, G. Gryniewich, J. Janesky, S. V. Pietambaram, N. D. Rizzo, J. M. Slaughter, K. Smith, J. J. Sun, and S. Tehrani, A 4-Mb toggle MRAM based on a novel bit and switching method, *IEEE Trans. Magn.* **41**, 132 (2005).
- [3] A. V. Khvalkovskiy, D. Apalkov, S. Watts, R. Chepulskii, R. S. Beach, A. Ong, X. Tang, A. Driskill-Smith, W. H. Butler, P. B. Visscher, D. Lottis, E. Chen, V. Nikitin, and M. Krounbi, Basic principles of STT-MRAM cell operation in memory arrays, *J. Phys. D: Appl. Phys.* **46**, 074001 (2013).
- [4] S. I. Kiselev, J. Sankey, I. Krivorotov, N. Emley, R. Schoelkopf, R. Buhrman, and D. Ralph, Microwave oscillations of a nanomagnet driven by a spin-polarized current, *Nature* **425**, 380 (2003).
- [5] W. H. Rippard, M. R. Pufall, S. Kaka, S. E. Russek, and T. J. Silva, Direct-current induced dynamics in Co₉₀Fe₁₀/Ni₈₀Fe₂₀ point contacts, *Phys. Rev. Lett.* **92**, 027201 (2004).
- [6] A. M. Deac, A. Fukushima, H. Kubota, H. Maehara, Y. Suzuki, S. Yuasa, Y. Nagamine, K. Tsunekawa, D. D. Djayaprawira, and N. Watanabe, Bias-driven high-power microwave emission from MgO-based tunnel magnetoresistance devices, *Nat. Phys.* **4**, 803 (2008).
- [7] S. Louis, O. Sulymenko, V. Tiberkevich, J. Li, D. Alois, O. Prokopenko, I. Krivorotov, E. Bankowski, T. Meitzler, and A. Slavin, Ultra-fast wide band spectrum analyzer based on a rapidly tuned spin-torque nano-oscillator, *Appl. Phys. Lett.* **113**, 112401 (2018).
- [8] D. Marković, N. Leroux, A. Mizrahi, J. Trastoy, V. Cros, P. Bortolotti, L. Martins, A. Jenkins, R. Ferreira, and J. Grollier, Detection of the microwave emission from a spin-torque oscillator by a spin diode, *Phys. Rev. Appl.* **13**, 044050 (2020).
- [9] S. Fukami and H. Ohno, Perspective: Spintronic synapse for artificial neural network, *J. Appl. Phys.* **124**, 151904 (2018).
- [10] T. Furuta, K. Fujii, K. Nakajima, S. Tsunegi, H. Kubota, Y. Suzuki, and S. Miwa, Macromagnetic simulation for reservoir computing utilizing spin dynamics in magnetic tunnel junctions, *Phys. Rev. Appl.* **10**, 034063 (2018).
- [11] M. Romera, P. Talatchian, S. Tsunegi, F. Abreu Araujo, V. Cros, P. Bortolotti, J. Trastoy, K. Yakushiji, A. Fukushima, H. Kubota, S. Yuasa, M. Ernoult, D. Vodenicarevic, T. Hirtzlin, N. Locatelli, D. Querlioz, and J. Grollier, Vowel recognition with four coupled spin-torque nano-oscillators, *Nature* **563**, 230 (2018).
- [12] A. Fukushima, T. Seki, K. Yakushiji, H. Kubota, H. Imamura, S. Yuasa, and K. Ando, Spin dice: A scalable truly random number generator based on spintronics, *Appl. Phys. Express* **7**, 083001 (2014).
- [13] E. A. Montoya, S. Perna, Y.-J. Chen, J. A. Katine, M. d'Aquino, C. Serpico, and I. N. Krivorotov, Magnetization reversal driven by low dimensional chaos in a nanoscale ferromagnet, *Nat. Commun.* **10**, 543 (2019).
- [14] A. S. Jenkins, L. S. E. Alvarez, P. P. Freitas, and R. Ferreira, Nanoscale true random bit generator based on magnetic state transitions in magnetic tunnel junctions, *Sci. Rep.* **9**, 15661 (2019).
- [15] A. Tulapurkar, Y. Suzuki, A. Fukushima, H. Kubota, H. Maehara, K. Tsunekawa, D. Djayaprawira, N. Watanabe, and S. Yuasa, Spin-torque diode effect in magnetic tunnel junctions, *Nature* **438**, 339 (2005).
- [16] P. N. Skirdkov and K. A. Zvezdin, Spin-torque diodes: From fundamental research to applications, *Ann. Phys.* **532**, 1900460 (2020).
- [17] G. Finocchio, R. Tomasello, B. Fang, A. Giordano, V. Puliafito, M. Carpentieri, and Z. Zeng, Perspectives on spintronic diodes, *Appl. Phys. Lett.* **118**, 160502 (2021).
- [18] X. Li, C. Zheng, Y. Zhou, H. Kubota, S. Yuasa, and P. W. Pong, Spin-torque diode with tunable sensitivity and bandwidth by out-of-plane magnetic field, *Appl. Phys. Lett.* **108**, 232407 (2016).
- [19] T. Zeng, Y. Zhou, K. Lin, P. Lai, and P. Pong, Spin-torque diode-based radio-frequency detector by utilizing tilted fixed-layer magnetization and in-plane free-layer magnetization, *IEEE Trans. Magn.* **51**, 1 (2015).
- [20] D. Bang, T. Taniguchi, H. Kubota, T. Yorozu, H. Imamura, K. Yakushiji, A. Fukushima, S. Yuasa, and K. Ando, Spin-torque diode spectrum of ferromagnetically coupled (FeB/CoFe)/Ru/(CoFe/FeB) synthetic free layer, *J. Appl. Phys.* **111**, 043305 (2012).
- [21] R. Matsumoto, H. Kubota, T. Yamaji, H. Arai, S. Yuasa, and H. Imamura, Spin-torque diode spectrum of a spin valve with a synthetic antiferromagnetic reference layer, *Jpn. J. Appl. Phys.* **53**, 123001 (2014).
- [22] A. A. Khudorozhkov, P. N. Skirdkov, K. A. Zvezdin, P. M. Vetroshko, and A. F. Popkov, Spin-torque diode frequency tuning via soft exchange pinning of both magnetic layers, *Phys. Rev. B* **96**, 214410 (2017).
- [23] N. E. Kulagin, P. N. Skirdkov, A. F. Popkov, K. A. Zvezdin, and A. V. Lobachev, Nonlinear current resonance in a spin-torque diode with planar magnetization, *Low Temp. Phys.* **43**, 708 (2017).
- [24] S. Tsunegi, K. Mizunuma, K. Suzuki, H. Imamura, S. Tamaru, M. Yoshimura, M. Sato, Y. Kono, H. Wado, A. Fukushima, H. Kubota, and S. Mizukami, Spin torque diode effect of the magnetic tunnel junction with MnGa free layer, *Appl. Phys. Lett.* **112**, 262408 (2018).
- [25] A. S. Jenkins, R. Lebrun, E. Grimaldi, S. Tsunegi, P. Bortolotti, H. Kubota, K. Yakushiji, A. Fukushima, G. De Loubens, O. Klein, S. Yuasa, and V. Cros, Spin-torque resonant expulsion of the vortex core for an efficient

- radiofrequency detection scheme, *Nat. Nanotechnol.* **11**, 360 (2016).
- [26] S. Tsunegi, T. Taniguchi, K. Yakushiji, A. Fukushima, S. Yuasa, and H. Kubota, Achievement of high diode sensitivity via spin torque-induced resonant expulsion in vortex magnetic tunnel junction, *Appl. Phys. Express* **11**, 053001 (2018).
- [27] P. N. Skirdkov, A. F. Popkov, and K. A. Zvezdin, Vortex spin-torque diode: The impact of dc bias, *Appl. Phys. Lett.* **113**, 242403 (2018).
- [28] S. Miwa, S. Ishibashi, H. Tomita, T. Nozaki, E. Tamura, K. Ando, N. Mizuochi, T. Saruya, H. Kubota, K. Yakushiji, T. Taniguchi, H. Imamura, A. Fukushima, S. Yuasa, and Y. Suzuki, Highly sensitive nanoscale spin-torque diode, *Nat. Mater.* **13**, 50 (2014).
- [29] B. Fang, M. Carpentieri, X. Hao, H. Jiang, J. A. Katine, I. N. Krivorotov, B. Ocker, J. Langer, K. L. Wang, B. Zhang, B. Azzerboni, P. K. Amiri, G. Finocchio, and Z. Zeng, Giant spin-torque diode sensitivity in the absence of bias magnetic field, *Nat. Commun.* **7**, 11259 (2016).
- [30] L. Zhang, B. Fang, J. Cai, M. Carpentieri, V. Puliafito, F. Garesci, P. K. Amiri, G. Finocchio, and Z. Zeng, Ultra-high detection sensitivity exceeding 105 v/w in spin-torque diode, *Appl. Phys. Lett.* **113**, 102401 (2018).
- [31] A. G. Buzdakov, P. N. Skirdkov, and K. A. Zvezdin, Magnetostatically induced easy-cone magnetic state tuning by perpendicular magnetic anisotropy in an unbiased spin-torque diode, *Phys. Rev. Appl.* **15**, 054047 (2021).
- [32] A. G. Buzdakov, P. N. Skirdkov, and K. A. Zvezdin, Easy-cone state in spin-torque diode under combined action of magnetostatics and perpendicular anisotropy, *J. Phys. D: Appl. Phys.* **55**, 115001 (2021).
- [33] O. Prokopenko, I. Krivorotov, E. Bankowski, T. Meitzler, S. Jaroch, V. Tiberkevich, and A. Slavin, Spin-torque microwave detector with out-of-plane precessing magnetic moment, *J. Appl. Phys.* **111**, 123904 (2012).
- [34] B. Fang, M. Carpentieri, S. Louis, V. Tiberkevich, A. Slavin, I. N. Krivorotov, R. Tomasello, A. Giordano, H. Jiang, J. Cai, Y. Fan, Z. Zhang, B. Zhang, J. A. Katine, K. L. Wang, P. K. Amiri, G. Finocchio, and Z. Zeng, Experimental demonstration of spintronic broadband microwave detectors and their capability for powering nanodevices, *Phys. Rev. Appl.* **11**, 014022 (2019).
- [35] M. Tarequzzaman, A. Jenkins, T. Böhnert, J. Borme, L. Martins, E. Paz, R. Ferreira, and P. Freitas, Broadband voltage rectifier induced by linear bias dependence in CoFeB/MgO magnetic tunnel junctions, *Appl. Phys. Lett.* **112**, 252401 (2018).
- [36] R. Tomasello, B. Fang, P. Artemchuk, M. Carpentieri, L. Fasano, A. Giordano, O. Prokopenko, Z. Zeng, and G. Finocchio, Low-frequency nonresonant rectification in spin diodes, *Phys. Rev. Appl.* **14**, 024043 (2020).
- [37] L. Zhang, B. Fang, J. Cai, W. Wu, B. Zhang, B. Wang, P. K. Amiri, G. Finocchio, and Z. Zeng, Enhanced broadband radio frequency detection in nanoscale magnetic tunnel junction by interface engineering, *ACS Appl. Mater. Interfaces* **11**, 29382 (2019).
- [38] P. Y. Artemchuk, O. Prokopenko, E. Bankowski, T. Meitzler, V. Tyberkevych, and A. Slavin, Rf signal detector and energy harvester based on a spin-torque diode with perpendicular magnetic anisotropy, *AIP Adv.* **11**, 025234 (2021).
- [39] T. Wada, T. Yamane, T. Seki, T. Nozaki, Y. Suzuki, H. Kubota, A. Fukushima, S. Yuasa, H. Maehara, Y. Nagamine, K. Tsunekawa, D. D. Djayaprawira, and N. Watanabe, Spin-transfer-torque-induced rf oscillations in CoFeB/MgO/CoFeB magnetic tunnel junctions under a perpendicular magnetic field, *Phys. Rev. B* **81**, 104410 (2010).
- [40] J. C. Sankey, Y.-T. Cui, J. Z. Sun, J. C. Slonczewski, R. A. Buhrman, and D. C. Ralph, Measurement of the spin-transfer-torque vector in magnetic tunnel junctions, *Nat. Phys.* **4**, 67 (2008).
- [41] H. Kubota, A. Fukushima, K. Yakushiji, T. Nagahama, S. Yuasa, K. Ando, H. Maehara, Y. Nagamine, K. Tsunekawa, D. D. Djayaprawira, N. Watanabe, and Y. Suzuki, Quantitative measurement of voltage dependence of spin-transfer torque in MgO-based magnetic tunnel junctions, *Nat. Phys.* **4**, 37 (2008).
- [42] C. Wang, Y.-T. Cui, J. Sun, J. Katine, R. Buhrman, and D. Ralph, Bias and angular dependence of spin-transfer torque in magnetic tunnel junctions, *Phys. Rev. B* **79**, 224416 (2009).
- [43] J. C. Slonczewski, Current-driven excitation of magnetic multilayers, *J. Magn. Magn. Mater.* **159**, L1 (1996).
- [44] L. Berger, Emission of spin waves by a magnetic multilayer traversed by a current, *Phys. Rev. B* **54**, 9353 (1996).
- [45] A. K. Zvezdin, K. A. Zvezdin, and A. V. Khvalkovskiy, The generalized Landau–Lifshitz equation and spin transfer processes in magnetic nanostructures, *Uspekhi Fizicheskikh Nauk* **178**, 436 (2008).